1 **Title: Pathobionts from chemically disrupted gut microbiota induce**
2 **insulin-dependent diabetes in mice**

3

4 **Authors:** Xin Yang[1], Zhiyi Wang[1], Junling Niu[1,3], Rui Zhai[1], Xinhe Xue[1], Guojun Wu[2],
5 Guangxun Meng[3], Huijuan Yuan[4], Liping Zhao[1,2†], Chenhong Zhang[1†]

6

7 **Affiliations:**

8 [1]State Key Laboratory of Microbial Metabolism and Ministry of Education Key Laboratory of Systems Biomedicine,
9 School of Life Sciences and Biotechnology, Shanghai Jiao Tong University, Shanghai 200240, China.

10 [2] Department of Biochemistry and Microbiology and New Jersey Institute for Food, Nutrition, and Health, School
11 of Environmental and Biological Sciences, Rutgers University, NJ 08901, USA.

12 [3] The Center for Microbes, Development and Health, CAS Key Laboratory of Molecular Virology & Immunology,
13 Institute Pasteur of Shanghai, University of Chinese Academy of Sciences, Shanghai 200031, China.

14 [4] Department of Endocrinology of Henan Provincial People's Hospital, People's Hospital of Zhengzhou University,
15 Zhengzhou, Henan 450003, China.

16

17 †Corresponding authors: Chenhong Zhang, email: zhangchenhong@sjtu.edu.cn
18   Liping Zhao, email: lpzhao@sjtu.edu.cn, liping.zhao@rutgers.edu
19   Huijuan Yuan, email: hjyuan@zzu.edu.cn

20
21

22   **ABSTRACT**

23   **Background:** Dysbiotic gut microbiome, genetically predisposed or chemically

24   disrupted, has been linked with insulin-dependent diabetes (IDD) including

25   autoimmune type 1 diabetes (T1D) in both humans and animal models. However,

26   specific IDD-inducing gut bacteria remain to be identified and their casual role in

27   disease development demonstrated via experiments that can fulfill Koch's postulates.

28   **Results**: Here, we show that novel gut pathobionts in the Muribaculaceae family,

29   enriched by a low-dose dextran sulfate sodium (DSS) treatment, translocated to the

30   pancreas and caused local inflammation, beta cell destruction and IDD in C57BL/6

31   mice. Antibiotic removal and transplantation of gut microbiota showed that this low

32   DSS disrupted gut microbiota was both necessary and sufficient to induce IDD.

33   Reduced butyrate content in the gut and decreased gene expression levels of an

34   antimicrobial peptide in the pancreas allowed for the enrichment of members in the

35   Muribaculaceae family in the gut and their translocation to the pancreas. Pure isolate of

36   one such members induced IDD in wildtype germ-free mice on normal diet either alone

37   or in combination with normal gut microbiome after gavaged into stomach and

38   translocated to pancreas.

39   **Conclusion:** The pathobionts that are chemically enriched in dysbiotic gut microbiota

40   are sufficient to induce insulin-dependent diabetes after translocation to the pancreas.

41   This indicates that IDD can be mainly a microbiome-dependent disease, inspiring the

42   need to search for novel pathobionts for IDD development in humans.

43

44   **Key Words:** insulin-dependent diabetes, gut pathobionts, Muribaculaceae
45

46 **Main text**

47 **Background**

48 Insulin-dependent diabetes (IDD) refers to a wide range of diabetic conditions

49 characterized by absolute insufficiency of insulin secretion [1]. The most prevalent type

50 of IDD is type 1 diabetes (T1D), which is an autoimmune condition that leads to

51 specific destruction of beta cells and complete loss of insulin-production [2]. Except

52 autoimmune T1D in which genetics may play a critical role, IDD can be caused by

53 environmental factors, such as treatment with immune checkpoint inhibitors, toxic

54 compounds, and infection etc. [3-5]. The rapid increase in the incidence of IDD in the

55 past three decades indicates that environmental factors, rather than genetics, may be the

56 main driver of such diseases [6]. However, the pathological mechanism on how such

57 environmental factors can induce IDD remain elusive.

58 It has been hypothesized that gut microbiota may work as a mediating factor in the

59 development of IDD [6]. This hypothesis has been supported mainly by studies on the

60 role of gut microbiota in the development of T1D in both animal models and human

61 cohorts [7]. Altered gut microbiota in connection to T1D has been reported in Finnish,

62 German, Italian, Mexican, American (Colorado) and Turkish children [8-10]. The

63 longitudinal functional profiling of the developing gut microbiome of infants in

64 TEDDY study showed that short-chain fatty acids (SCFAs) from fermentation of gut

65 microbiota have protective effects in early-onset human T1D [8]. Studies have shown

66 that the gut microbiota and its metabolites contribute to the development of T1D in

67 NOD mice through regulating toll-like receptor-dependent signaling [11, 12], sex

68 hormone-related pathways [13], IL-17 related mucosal immune reactions [14, 15], and

69 pancreatic production of antimicrobial peptides [16]. However, germ-free mice derived

70 from NOD mice can still develop T1D, indicating that the gut microbiota is not essential

71 for the development of T1D in this animal model [13]. The development of IDD in

72 mice treated with toxic compounds, such as streptozotocin (STZ), has also been

73 associated with gut microbiota dysbiosis. Interestingly, the removal of the gut

74 microbiota by an antibiotic cocktail blocked IDD induction by STZ, showing that the

75 gut microbiota may be indispensable for this chemically-induced IDD [7]. However,

76 specific members of the dysbiotic gut microbiota which may drive IDD, and the

77 associated etiological mechanisms remain to be elucidated.

78   Many toxic compounds have been shown to disrupt the gut microbiota and

79 aggravate inflammation-related diseases, including metabolic diseases [17]. Notably,

80 dextran sulfate sodium (DSS), a compound with very low bioavailability, has been well

81 known for its effect on disrupting the gut microbiota and inducing acute colitis at a high

82 dose (2-3%) and chronic colitis at a low dose (0.5-1%) when administered via drinking

83 water in mice [18-20]. To explore how an even lower level of DSS would affect the gut

84 microbiota and host health, we reduced the dose to 0.2%. We serendipitously found that

85 the mice did not show inflammation or impaired barrier function in their gut; instead,

86 they developed IDD with pancreatic beta cells significantly destructed. We identified

87   and isolated one of the pathobionts in family Muribaculaceae which was enriched in

88   the low DSS-disrupted gut microbiota and confirmed that this single pathobiont is

89   sufficient to induce the initiation and progression of IDD in germfree mice. This study

90   indicates that IDD can be a microbiome-dependent disease, inspiring the search of such

91   novel pathobionts for IDD development in humans.

92   **Methods**

93   **<u>Animal Trials</u>**

94   ***Mice***

95   Five-week-old SPF male mice (C57BL/6) were obtained from SLAC Inc. (Shanghai,

96   China) and kept under SPF environment at the animal facility of Shanghai Jiao Tong

97   University, Shanghai, China. Mice (five mice/cage) were housed in IVC system cages

98   (Dimensions 325 × 210 × 180 mm; Suzhou Fengshi Laboratory Animal Equipment Co.,

99   Ltd). The mice were fed with a sterilized normal chow diet (10% energy from fat; 3.25

100   kcal/g; 1010009, SLAC) and were housed in a room maintained at $22.0 \pm 1°C$ with 30-

101   70% humidity, with a 12 h light/dark phase cycle (lights on at 07:00 am).

102   Eight-week-old of germ-free male C57BL/6 mice were maintained in flexible-film

103   plastic isolators at the Laboratory Animal Center of the SLAC Inc. (Shanghai, China).

104   The mice were fed a sterilized normal chow diet (10% energy from fat; 3.25 kcal/g;

105   P1103F-50, SLAC). The mice were housed in a room maintained at $22.0 \pm 1°C$ with

106 30-70% humidity with a 12 h light/dark phase cycle (lights on at 06:00 am).

107 Surveillance for bacterial contamination was performed by periodic bacteriological

108 examinations of feces, food and padding. Detailed operations of surveillance for

109 bacterial contamination were consistent with previous work [21].

110 ***Animal Trials***

111 **Trial-1:** After one-week of acclimation, the mice were randomly assigned to 2 groups:

112 (i) NC group (n = 10), control mice provided pure drinking water for feeding 12 weeks;

113 (ii) DSS group (n = 10), mice treated with 0.2% (w/v) DSS (0216011080, MP

114 Biomedicals, USA) to drinking water for feeding 12 weeks. Independently repeated

115 trials were performed three times.

116 **Trial-2:** After one-week of acclimation, a cocktail of antibiotics (0.5 g/L of

117 vancomycin, 1 g/L of ampicillin, 1 g/L of neomycin, 1 g/L of metronidazole) was

118 introduced in drinking water [22]. For 5 weeks. The mice were then randomly assigned

119 to 2 groups: (i) ABX group (n = 10), antibiotic cocktail-treated mice provided pure

120 drinking water for 12 weeks; (ii) ABX+DSS group (n = 8), antibiotic cocktail-treated

121 mice with 0.2% (w/v) DSS added to drinking water for 12 weeks. During the 12 weeks,

122 both groups continued to have the antibiotic cocktail in their drinking water.

123 **Trial-3:** After one-week of acclimation, the antibiotic cocktail was introduced in

124 drinking water for 5 weeks. The mice were then randomly assigned to 2 groups: (i)

125 FM_{NC} group (n = 10), antibiotic cocktail-treated mice inoculated with the fecal

126   inoculum from mice in the NC group and provided pure water for feeding 20 days; (ii)

127   FM_{DSS} group (n = 10), antibiotic cocktail-treated mice inoculated with the fecal

128   inoculum from mice in the DSS group and provided pure water for feeding 20 days.

129   The oral gavage was performed once a day for 3 times (Day 0, Day 1 and Day 4). Each

130   mouse was given 200 µL of inoculum every time.

131   **Trial-4:** After one-week of acclimation, the antibiotic cocktail was introduced in

132   drinking water for 5 weeks. The mice were then randomly assigned to 2 groups: (i)

133   FM_{NC} group (n = 10), antibiotic cocktail-treated mice inoculated with the fecal

134   inoculum from mice in the NC group and provided pure drinking water for 20 days; (ii)

135    $FM_{NC+Muri}$ group (n = 10), antibiotic cocktail-treated mice inoculated with a mixture of

136   the fecal inoculum of the NC group and the MF 13079 strain and provided pure drinking

137   water for 20 days. The oral gavage was performed once a day for 3 times (Day 0, Day

138   1 and Day 4). Each mouse was given 200 µL of fecal inoculum every time in FM_{NC}

139   group; and each mouse was given 100 µL fecal inoculum and 100 µL bacterial

140   suspension in $FM_{NC+Muri}$ group.

141   **Trial-5:** The germ-free mice were randomly assigned to two groups and each group

142   was kept in an individual plastic isolator. (i) Akk group (n = 12), germ-free mice

143   inoculated with the *Akkermansia muciniphila* strain 139 and provided pure drinking

144   water for 14 days; (ii) Muri group (n = 11), germ-free mice inoculated with the MF

145   13079 strain and provided pure drinking water for 14 days. The oral gavage was

146   performed once a day for 2 consecutive days. Each mouse was given 200 µL of bacterial

147   suspension every time.

Preparation of Inoculum

Preparation of inoculum from mice feces

150   Fresh fecal samples from each mouse in NC and DSS groups (in the 12th week of Trial-

151   1) were collected. The fecal samples in the same group were mixed in anaerobic sterile

152   Ringer working buffer (9 g/L of sodium chloride, 0.4 g/L of potassium chloride, 0.25

153   g/L of calcium chloride dehydrate and 0.05% (w/v) L-cysteine hydrochloride) in an

154   anaerobic chamber (80% N_2 :10% CO_2 :10% H_2) [23], and   diluted to 50 times. Then

155   the suspensions were added with 20% (w/v) skim milk (LP0031, Oxoid, UK) and the

156   final fecal suspensions were diluted to 100 times. The fecal suspensions were preserved

157   at − 80 °C until inoculation.

Preparation of bacterial suspensions

159   *Akkermansia muciniphila* strain 139 was cultured in a synthetic medium [24] and

160   Muribaculaceae strain MF13079 was cultured in a modified MPYG medium (Table S1).

161   The harvested bacterial cells were washed twice with PBS (pH 7.4) and resuspended in

162   PBS (pH 7.4) and added with equal volume of 20% skim milk to a density of 10^9

163   cells/ml. The bacterial suspensions were stored at − 80 °C until inoculation.

Glucose Tolerance Test and Estimation of Insulin Sensitivity

Oral glucose tolerance test (OGTT)

Mice were fasted for 6 h and baseline blood glucose levels were measured with an Accu-Check Performa blood glucose meter (Roche, USA) using blood collected from the tail vein. After administration of glucose (2.0 g/kg body weight) via oral gavage, blood glucose levels were measured at 15, 30, 60, and 120 min. Serum insulin levels were also measured by ELISA kit (90080, Crystal Chem, USA) at 0, 15, 30, 60 min after glucose challenge.

Insulin tolerance test (ITT)

Six hours fasted mice were injected intraperitoneally with 1.0 U insulin/kg body weight (Novolin, Novo Alle, Denmark). Blood glucose was then measured at 0, 15, 30, 60, and 120 min after injection with the blood glucose meter (Roche, USA).

In vivo **Intestinal Permeability Assay**

Intestinal permeability was measured based on the permeability to 4000 Da-FITC-dextran in plasma (DX-4000-FITC) (46944; Sigma-Aldrich, St. Louis, Missouri, USA) as previously described [25]. Briefly, after fasting for 6 h, the mice were administered with DX-4000-FITC (500 mg/kg body weight, 125 mg/mL) by oral gavage. After 4 h, blood plasma collected from the tip of the tail vein was diluted with equal volume of PBS (pH 7.4) and analyzed for DX-4000-FITC concentration with a fluorescence spectrophotometer (HTS-7000 Plus-plate-reader; Perkin Elmer, Wellesley, Massachusetts, USA) at an excitation wavelength of 485 nm and emission wavelength

185   of 535 nm. A standard curve was obtained by diluting FITC-dextran in non-treated

186   plasma diluted with PBS (1:3 v/v).

187   **Energy Assessment of Feces**

188   *Fecal output measurement*

189   Mice were placed in a clean cage individually and feces were collected for 24 h. Dry

190   weights were taken after fecal pellets were incubated at 65°C in an oven for 24 h (JC101,

191   Shanghai Chengshun Instrument & Meter Co., Ltd, Shanghai, China).

192   *Bomb calorimetry*

193   Bomb calorimetry was performed on dried fecal pellets. Gross energy content was

194   measured using an isoperibol bomb calorimeter (C6000, IKA, Germany). The

195   calorimeter energy equivalent factor was determined using benzoic acid standards.

196   **Triglycerides and Cholesterol Measurement**

197   Serum cholesterol and triglycerides were quantified with colorimetric kits (A111-1-1-

198   1 and A110-1-1, respectively) from Nanjing Jiancheng Bioengineering Institute

199   (Nanjing, China).

200   Frozen liver sample was homogenized in a corresponding volume (1:9, w:v) of

201   homogenizing buffer (pH 7.4, 0.01 mol/L Tris-HCl, 0.1 mmol/L EDTA-2Na, 0.8%

202   NaCl). The supernatant was collected after centrifugation for 25 min at 2,000×g and

203   4 °C. Cholesterol and triglycerides in homogenized tissue were quantified by

204   colorimetric kits from Nanjing Jiancheng Bioengineering Institute (Nanjing, China).

205   Tissue homogenized total protein was measured with the Protein Quantification Kit

206   (20202ES76; Yeasen Biotechnology Ltd., Shanghai, China).

207   **Amylase and Lipase Measurement**

208   Serum amylase and lipase were quantified with colorimetric kits (C016-1-1 and A054-

209   2-1, respectively) from Nanjing Jiancheng Bioengineering Institute (Nanjing, China).

210   **Fecal Lipocalin-2 Detection**

211   Fecal lipocalin-2 content was quantified with a Lipocalin-2/NGAL Quantikine ELISA

212   kit (DLCN20, R&D Systems).

213   **mRNA Expression of Genes Related with Gut Barrier Integrity in the Colon**

214   The total RNA of colons was extracted using the RNeasy Plus Universal Tissue Mini

215   Kit (73404, Qiagen, Duesseldorf, Germany). The RNA was reverse-transcribed to

216   cDNA using the SuperScript™ III First-Strand Synthesis (18080051, Invitrogen, Calif.,

217   USA). RT-qPCR was performed with the Light Cycler 96 (Roche, Geneva, Switzerland)

218   using iQ SYBR Green Supermix (170-8882AP, BIO-RAD, CA, USA). The PCR

219   conditions were 95°C for 3 min, followed by 40 cycles of 95°C for 20 s, 56°C for 30 s,

220   and 72°C for 30 s, and plate reads for 5 s. Gene expression levels were determined using

221   the comparative $\Delta\Delta C_T$ method ($2^{-\Delta\Delta C_T}$ method), with the β-actin gene serving as the

222   housekeeping gene. Forward (F) and reverse (R) primer sequences are as follows:

223 *β-actin*, F-CCTTCTTGGGTATGGAATCCTGTG, and R-

224 CAGCACTGTGTTGGCATAGAGG;

225 *Tjp*1, F-ACCCGAAACTGATGCTGTGGATAG, and R-

226 AAATGGCCGGGCAGAACTTGTGTA;

227 *Cldn*1, F-GATGTGGATGGCTGTCATTG, and R-CCTGGCCAAATTCATACCTG;

228 *Muc*1, F-TACCCTACCTACCACACTCACG, and R-

229 CTGCTACTGCCATTACCTGC;

230 *Muc*2, F-CACCAACACGTCAAAAATCG, and R-GGTCTCTCGATCACCACCAT;

231 *Muc*3, F-CTTCCAGCCTTCCCTAAACC, and R-TCCACAGATCCATGCAAAAC;

232 *Muc*4, F-GAGAGTTCCCTGGCTGTGTC, and R-GGACATGGGTGTCTGTGTTG;

233 *Zo*-1, F-ACCCGAAACTGATGCTGTGGATAG, and R-

234 AAATGGCCGGGCAGAACTTGTGTA;

235 *Occludin*, F- ATGTCCGGCCGATGCTCTC, and R-

236 TTTGGCTGCTCTTGGGTCTGTAT.

237 **Histopathology**

238 Fresh epididymal fat pads were fixed with 4% paraformaldehyde for 48 h, embedded

239 in paraffin, sectioned, and stained with hematoxylin and eosin (H&E) (G1003; Wuhan

240 Servicebio technology Ltd., Wuhan, China). Digital images of sections were acquired

241 with a Leica DMRBE microscope. Adipocyte sizes were assessed using Image Pro Plus

242   v6.0 (Media Cybernetics Inc., Silver Springs, MD, USA). For each mouse, mean areas

243   of adipocytes were determined in five discontinuous scans under ×200 magnification.

244   Fresh liver tissues were fixed with 4% paraformaldehyde for 48 h, embedded in

245   paraffin, sectioned, and stained with hematoxylin and eosin (H&E) (G1003; Wuhan

246   Servicebio technology Ltd., Wuhan, China). Digital images of sections were acquired

247   with a Leica DMRBE microscope. For Oil Red O staining of liver sections, liver tissues

248   were fixed in 4% paraformaldehyde for at least 48 h, embedded in optimal cutting

249   temperature (OCT) compound (4583; CellPath Ltd., Newtown, Powys, UK) and frozen

250   at −20 °C. Sections were stained with Oil Red O (O0625; Sigma-Aldrich Ltd., St. Louis,

251   MO, USA). Digital images of sections were acquired with a Leica DMRBE microscope.

252   Fresh pancreatic tissues were fixed with 4% paraformaldehyde for 48 h, embedded

253   in paraffin, sectioned, and stained with hematoxylin and eosin (H&E) (G1003; Wuhan

254   Servicebio technology Ltd., Wuhan, China). Digital images of sections were acquired

255   with a Leica DMRBE microscope. pancreas islet number were assessed using Image

256   Pro Plus v6.0 (Media Cybernetics Inc., Silver Springs, MD, USA). Histological

257   analysis of pancreatitis was determined by one observer who was blinded to the

258   treatment group. Scores of pancreatitis severity was assessed as described

259   previously[26].

260   **Immunofluorescence Observation of Insulin in the Pancreas**

261 Fresh pancreatic tissues were fixed with 4% paraformaldehyde and then embedded in

262 paraffin. Subsequently, 4 μm sections were blocked with 5% bovine albumin (BSA),

263 and stained overnight with anti-insulin pAb (1:500, Abcam, ab7842) at 4°C. After

264 washing, anti-pig-AlexaFluor488 secondary antibody as the second-step reagents were

265 applied. The sections were incubated for 15 min at room temperature in the dark. Nuclei

266 were stained with DAPI (G1012, Servicebio). Digital images of sections were acquired

267 with a Leica DMRBE microscope after completely rinsing with sterile PBS. The

268 insulin-positive area of each section was counted with Image Pro Plus v6.0 (Media

269 Cybernetics Inc., Silver Springs, MD, USA).

Immunohistochemical Analysis of ZO-1 and Occludin in the Colon

271 After deparaffinization and processing for antigen retrieval, the blank colon sections

272 were incubated overnight at room temperature with anti-rabbit ZO-1 antibody (1:500,

273 catalog no. GB11195; Servicebio, China) and Occludin antibody (1:200, catalog no.

274 GB11149; Servicebio) separately. Sections were then incubated with anti-rabbit IgG

275 secondary antibody (KPL, MA, USA) for 50 min at room temperature. After washing

276 with PBS, the DAB Envision kit (catalog no. K5007; Dako, Copenhagen, Denmark)

277 was used to develop color; ZO-1 and Occludin appear brown, while nuclei are blue.

278 Images of each colon section were obtained in tripartite by experienced staff who were

279 blind to the experiment under ×200 magnification using a Leica DMRBE microscope

280 and were analyzed using Image Pro Plus 6.0, according to the method previously

281 described [27]. The integrated optical density (IOD) values were log10 transformed.

282 **Flow Cytometry Evaluation of Subtypes of Leukocytes in the Pancreas**

283 Fresh pre-cut pancreatic tissue (2×2 mm) were digested with a solution of collagenase

284 P in HBSS-1% HEPES (0.75 mg/mL, Roche) at 37°C for 7 min with shaking. Digestion

285 was stopped by adding HBSS-10% FCS 1% EDTA followed by extensive washes by

286 FACS buffer (1×PBS pH7.2, 0.5% BSA, 2mM EDTA). The suspensions were filtered

287 through 100 μm cell strainer (352360, FALCON, USA). Suspensions were transfer into

288 Polystyrene Round-Bottom Tube (352052, FALCON, USA) followed by centrifugation

289 at 400×g at 4°C for 5 min. To ensure single cell bioactivity, it was necessary to disperse

290 the cells quickly after discarding the supernatant. 500 μL FACS buffer was added to re-

291 suspend cells. The wash step was repeated twice to get a single cell suspension. Non-

292 specific binding was blocked with FcR blocking antibody (anti-mouse CD16/32,

293 553142, BD Pharmingen) before surface staining with the following mAbs: Anti-mouse

294 CD45.2 (563051, BD Horizon), Anti-mouse-CD3e (562600, BD Horizon), Anti-

295 mouse-CD4 (553653, BD Pharmingen), Anti-mouse-CD8a (551162, BD Pharmingen),

296 Anti-mouse-F4/80 (12-4801-82, eBioscience). Single cell suspension was washed

297 twice as described above by 500 μL FACS buffer. Intracellular staining was carried out

298 after fixation and permeabilization (00-5523-00, eBioscience) with the following

299 antibodies: Anti-mouse Foxp3 (77-5775-40, eBioscience), Anti-mouse-IL-17A (12-

300 7177-81, eBioscience). Dead cells were excluded with a fixable viability dye (65-

301 086514, Invitrogen, USA). The fluorescence was examined on an Flowcytometer (BD

302 LSRFortessa, Becton, Dickinson and Company, USA).

Sequence-guided Bacteria Isolation

Fresh fecal samples from DSS group were collected and mixed in anaerobic sterile Ringer working buffer in an anaerobic workstation (Don Whitley Scientific Ltd, Shipley, UK). The 10^5 diluted suspension with Ringer working buffer was placed onto 46 medium plates (Table S1) and incubated under anaerobic condition (80% N_2, 10% CO_2, and 10% H_2) at 37°C for 7 days. The 16S rRNA gene of each colony was obtained using the primers 27-F (AGAGTTTGATCCTGGCTCAG) and 1492-R (GGTTACCTTGTTACGACTT). The obtained 16S rRNA sequences were sequenced and aligned with the ASVs in Muribaculaceae enriched in the gut of DSS-treated mice. One Muribaculaceae strain (MF13079) was isolated using a previously reported MPYG medium [28] which was modified by adding 3% fetal bovine serum (FBS, GIBCO, 10099-141). The Muribaculaceae strain MF13079 16S rRNA sequence was aligned with the GenBank. All the 16S rRNA sequence of the isolated strains in the family Muribaculaceae and the 16S rRNA sequence of the representative strains in other families of the phylum Bacteroidetes were selected to build a phylogenetic tree by using the Neighbor-Joining method in MEGA 6.

Whole-Genome Sequencing and Analysis of MF13079

Whole-genome DNA of Muribaculaceae strain MF13079 was extracted with QIAamp BiOstic Bacteremia DNA Kit (12240-50, Qiagen, USA) and sequenced with the Oxford@ Nanopore PromethION platform (performed by Nextomics Biosciences,

323   Wuhan, China). Subreads of the sequence were assembled into a single complete

324   chromosome using the HGAP 2.3.0 pipeline [29].

325   The genome sequence of Muribaculaceae strain MF13079 was adjusted to start

326   with the replicational origin (location of *DnaA*) for comparison. Protein-coding

327   sequences (CDSs), tRNAs, and rRNAs were predicted and annotated using the Prokka

328   1.12 pipeline (Table S2) [30]. Functional annotation of genes related with flagella-

329   synthesis in the CDSs of MF13079 was performed using the Kyoto Encyclopedia of

330   Genes and Genomes (KEGG) database.

331   **Microbiota Profiling in Tissues**

332   *DNA extraction of microorganisms in tissues*

333   Pre-cut pancreatic tissue (5×5 mm) and mesenteric lymphatic nodes (MLNs) were

334   homogenized using a sterile pestle in a sterile mortar under liquid nitrogen as the media.

335   Homogenate was used for DNA extraction by QIAamp Pro DNA Kit (51804, Qiagen,

336   Duesseldorf, Germany). Sterile DNA-free water was used as negative controls.

337   *Bacterial load in the pancreas and mesenteric lymphatic nodes (MLNs)*

338   Nested PCR was used in this situation. The 16S rRNA gene was first amplified using

339   the   primers   27-F   (AGAGTTTGATCCTGGCTCAG)   and   1492-R

340   (GGTTACCTTGTTACGACTT). PCR was performed in a volume of 25.0 μl with 10

341   ng DNA template, 1 μl of each primer (12.5 μM), 2.5 μl of 10× PCR buffer, 0.3 μl of

342   Taq polymerase (TaKaRa), 1 μl of dNTP mix (2.5 mM). The reaction conditions

343   consisted of initial denaturation at 94 °C for 5 min; 25 cycles of 94 °C for 30 s, 55 °C

344   for 30 s and 72 °C for 90 s; and a final extension step for 10 min at 72 °C. Subsequently,

345   a 466 bp length sequence located in 16S rRNA gene was used for quantitative PCR

346   through the primers Uni331F (TCCTACGGGAGGCAGCAGT) and Uni797R

347   (GGACTACCAGGGTATCTAATCCTG TT) [31]. Briefly, qPCR was performed with

348   the Light Cycler 96 (Roche, Geneva, Switzerland) using iQ SYBR Green Supermix

349   (170-8882AP, BIO-RAD, CA, USA). The PCR conditions were 95°C for 3 min,

350   followed by 40 cycles of 95°C for 15 s, 60°C for 60 s and plate read for 5 s at 80°C. A

351   whole-length 16S rRNA gene of an *Akkermansia muciniphila* strain derived from mice

352   intestine was used to plot a standard curve to calculate the copies of 16S rRNA genes

353   in the samples.

354   ***Fluorescence in situ hybridization (FISH) of 16S rRNA in the pancreas***

355   The EUB338 16S rRNA probe labeled with the fluorophore Cy3 (extinction

356   wavelength, 555 nm; emission wavelength, 570 nm; Servicebio, China) was used to

357   detect the bacterial colonization within mouse pancreatic tissues by FISH. Nuclei were

358   stained with DAPI (G1012, Servicebio). Fluorescence microscopic analysis was

359   conducted with Nikon Eclipse 90i confocal microscope (Nikon, Melville, NY) using a

360   Cy3 labeled-probe at 1μM as described [32-34].

361   ***Pancreatic microbiota analysis by sequencing of V3-V4 region in 16S rRNA gene***

362   The 16S rRNA gene was first amplified from total DNA of pancreatic tissue using the

363   primers   27-F   (AGAGTTTGATCCTGGCTCAG)   and   1492-R

364   (GGTTACCTTGTTACGACTT). The PCR products were used as a template, a

365   sequencing library of the V3-V4 region of the 16S rRNA gene was constructed

366   following the manufacturer's instructions (Part # 15044223Rev.B; Illumina Inc., San

367   Diego, CA, USA) with improvement as previously described [20], and sequenced on

368   the Illumina MiSeq platform (Illumina, Inc., San Diego, CA, USA). The negative

369   controls from DNA extraction step were amplified and sequenced. Sterile DNA-free

370   water was also used as template for PCR in sequencing library preparation and then

371   sequenced.

372   The raw paired-end reads were processed and analyzed using the Quantitative

373   Insights into Microbial Ecology 2 (QIIME2, v2019.01) platform [28]. Demultiplexed

374   sequence data was imported into QIIME2, adapters and primers were trimmed.

375   Amplicon sequence variants (ASVs) from each sample was inferred by using the

376   DADA2 pipeline [35] for filtering, dereplication, sample inference, merging of paired-

377   end reads and chimera identification. In the process of running the DADA2 pipeline,

378   based on the quality profile of the data, forward and reverse reads were trimmed

379   accordingly to ensure that the median quality score for each position is above 32.

380   Potential reagent and environmental contaminations were identified using "decontam

381   (v.1.2.1)" package in R (v3.4.4) based on the frequency of the ASV in the negative

382   controls with threshold set at 0.5 [36]. The identified contaminants were removed from

383 dataset. After removing contaminants, all samples were rarefied to 6,000 reads per

384 sample for downstream analysis.

385 **Gut Microbiota Profiling**

386 The bacterial DNA extraction from fecal samples of mice was performed as previously

387 described [37]. A sequencing library of the V3-V4 region of the 16S rRNA gene was

388 constructed following the manufacturer's instructions (Part # 15044223Rev.B; Illumina

389 Inc., San Diego, CA, USA) with improvement as previously described [20], and

390 sequenced on the Illumina MiSeq platform (Illumina, Inc., San Diego, CA, USA).

391 The raw paired-end reads were processed and analyzed using the QIIME2.

392 Demultiplexed sequence data was imported into QIIME2, adapters and primers were

393 trimmed. ASVs from each sample was inferred by using the DADA2 pipeline for

394 filtering, dereplication, sample inference, merging of paired-end reads and chimera

395 identification. In the process of running the DADA2 pipeline, based on the quality

396 profile of the data, forward and reverse reads were trimmed accordingly to ensure that

397 the median quality score for each position is above 32. The taxonomy of all ASVs were

398 annotated by SILVA (v132) reference database [38]. All samples were rarefied to

399 10,000 reads per sample for downstream analysis. Principal coordinate analysis (PCoA)

400 of ASVs based on Bray-Curtis distance was performed using QIIME2. Subsequently

401 the statistical significance was assessed using permutational multivariate analysis of

402 variance (PERMANOVA) with 9,999 permutations and *P* values were adjusted for

403 multiple comparison with Benjamini-Hochberg method [39].

404 Sparse partial least-squares discriminant analysis (sPLS-DA) models [40] were

405 established to identify specific ASVs that contributed to the segregation of gut

406 microbial structure in NC and DSS mice using "mixOmics (v6.3.1)" package [41] in R

407 (v3.4.4). Centered log ratio (CLR) transformations of the relative abundance of ASVs

408 were implemented in sPLS-DA models. The optimal classification performances of the

409 sPLS-DA models were estimated by the perf function using 5-fold cross-validation with

410 the smallest balanced error rate.

411 **Statistical analysis**

412 Data in point plots and bar plots, horizontal lines indicate Mean ± S.E.M. Statistical

413 significance was assessed by Student's two-tailed t test using GraphPad Prism (version

414 8), with *P* values of <0.05 considered significant.

415 **Results**

416 **Low-dose DSS induced gut microbiota-dependent IDD**

417 To determine how a lower than usual dose of DSS would affect gut microbiota

418 and host health, we randomized 6-week-old C57BL/6 mice into a treatment group with

419 0.2% DSS in the drinking water or a control group with no any DSS intake. Compared

420 with control mice, the mice that received 12 weeks of low dose DSS treatment showed

421   a significant increase in blood glucose levels and decrease in insulin levels in oral

422   glucose tolerance test (OGTT) (Figure 1A and 1B). Moreover, the low dose DSS-

423   treated mice and control did not differ in blood glucose levels in an insulin tolerance

424   test (ITT), indicating that the low dose DSS-treated group did not develop insulin

425   resistance (Figure 1C). Compared with the control mice, low dose DSS-treated mice

426   had significantly decreased insulin expression in the pancreas (Figure 1D). We also

427   found that the fasting C-peptide level in serum was significantly lower in mice with low

428   dose DSS treatment than the control mice, demonstrating that the abnormal high

429   glucose level was due to low insulin production and secretion (Figure S1). The low

430   dose DSS-treated mice showed islet destruction in the pancreas (Figure 1E). These mice

431   also showed mild pancreatitis, as indicated by histological characteristics, such as

432   inflammatory cell infiltration and edema in the pancreas (Figure 1F), and an increase

433   in serum amylase levels (Figure S2). The DSS-treated mice had significantly higher

434   daily food and water intake than the control mice starting from the 8th week of treatment

435   (Figure S3). However, the energy consumption, body weight gain, and lipid metabolism

436   did not differ between low dose DSS treatment and control throughout the study period

437   (Figures S4). Thus, the treatment with 0.2% DSS in drinking water induced IDD in

438   wild-type C57BL/6 mice.

439   However, unlike higher doses DSS [42], this low dose DSS treatment did not

440   induce colitis or gut barrier impairment in mice. H&E-stained histological sections of

441   colon tissue showed that there were no structural changes of epithelium in the mice

442   with 0.2% DSS in drinking water compared with the control (Figure S5). The

443   fluorescein isothiocyanate (FITC)-dextran test, levels of mRNA expression of 8

444   different genes related with gut barrier integrity and immunohistochemical staining of

445   Occludin and Zo-1 showed no significant difference in intestinal permeability in mice

446   with or without 0.2% DSS treatment (Figure S5). Moreover, the fecal lipocalin-2

447   content, a biomarker for gut inflammation, had no significant difference between the

448   0.2% DSS-treated and control mice (Figure S5).

449   Although the dose of DSS used in our model was much lower than the dose needed

450   to induce colitis [18], the gut microbiota structure in the low dose DSS-treated mice

451   was significantly shifted away from the control, as shown by its reduced richness

452   (Figure 1G) and significant difference in principal coordinate analysis (PCoA) score

453   plot of Bray-Curtis distance based on the amplicon sequence variants (ASVs) of the

454   16S rRNA gene V3-V4 region (P=0.001 by permutational multivariate analysis of

455   variance (PERMANOVA) test with 999 permutations, Figure 1H). Thus, the

456   development of low dose DSS-induced IDD in mice was accompanied by significant

457   changes in the gut microbiota without inducing colitis.

458   To find out whether the disrupted gut microbiota was necessary for the

459   development of IDD induced by low dose DSS, we treated the adult C57BL/6 mice

460   with a cocktail of antibiotics for 5 weeks that depleted the gut microbiota by more than

461   99% (Figure S6). We then introduced 0.2% DSS into the drinking water of the mice

462   which were continuously treated with the antibiotic cocktail. Under the gut microbiota-

463   depleted condition, DSS-treated (ABX+DSS) and control (ABX) mice had

464   indistinguishable glucose metabolism, insulin secretion and histology in the pancreas

465   (Figure 2, Figure S2). Thus, the removal of the gut microbiota abolished the low dose

466   DSS-induced IDD in mice, indicating that the gut microbiota is essential for the disease

467   induction. To test if the DSS-disrupted gut microbiota is sufficient to induce IDD, we

468   transferred feces from control and 0.2% DSS-treated C57BL/6 mice to antibiotic-

469   treated mice [43]. The recipient mice were denoted FM_{NC} and FM_{DSS} mice, respectively.

470   Two weeks after the transplantation, the FM_{DSS} and FM_{NC} mice developed a gut

471   microbiota more similar to those of their donor (Figure S7). Moreover, the FM_{DSS} mice

472   showed significantly higher blood glucose level, lower insulin secretion, more beta cell

473   destruction and more signs of pancreatitis compared with the FM_{NC} mice, even though

474   all the recipient mice were provided pure water during the trial (Figure 2, Figure S2).

475   This result demonstrates that the gut microbiota treated by low dose DSS is sufficient

476   to induce IDD in mice. Thus, this chemically induced IDD in mice was causally

477   mediated by the gut microbiota which was disrupted by the low dose DSS treatment.

478   **Translocation of candidate gut pathobionts to the pancreas promoted local**

479   **inflammation**

480   To identify key members of the gut microbiota enriched by the low dose DSS which

481   may causally contribute to IDD development, we first identified ASVs in the gut

482   microbiota which showed significant differences between the 0.2% DSS-treated and

483   control mice by sparse partial least squares discriminant analysis (sPLS-DA) (Figure

484   3A and Figure S8). Notable changes were observed in the family Muribaculaceae

485   (phylum Bacteroidetes), a major but understudied mouse taxon [44]. Specifically, 4

486   ASVs in this family were enriched, while 6 ASVs were depleted (Figure 3A). On the

487   other hand, ASVs associated with potential butyrate producers, such as 2 ASVs in the

488   genus *Eubacterium*, were decreased (Figure 3A). Butyrate content was significantly

489   lower in DSS-treated than in control mice (Figure 3B). The butyrate content was also

490   significantly lower in FM_{DSS} mice compared with that in FM_{NC} mice (Figure 3B).

491   Reduced diversity of butyrate-producing bacteria and lower gut butyrate content have

492   been linked with overgrowth of pathobionts [45]. We hypothesized that the 4 ASVs in

493   the family Muribaculaceae enriched by low dose DSS may represent candidate

494   pathobionts for IDD development.

495   Translocation of gut pathobionts to pancreas has bene linked with a few disease

496   conditions [46]. We hypothesized that the candidate pathobionts enriched in low dose

497   DSS disrupted gut microbiota may translocate to pancreas and induce IDD. Indeed,

498   qPCR and fluorescence in situ hybridization (FISH) targeting the 16S rRNA gene

499   showed that the bacterial load was significantly higher (by at least one order of

500   magnitude) in the pancreas of the low dose DSS-treated and FM_{DSS} mice than in that of

501   their respective controls (Figures 3C and 3D, Figure S9 and S10). Absolute abundance

502   by multiplying the relative abundance from sequencing the V3-V4 region of the 16S

503   rRNA gene of the microbiota with qPCR derived total copy number of 16S rRNA genes

504   in the pancreas showed that the most abundant bacteria in the pancreas of control mice

505   belonged to the family Akkermansiaceae, but the microbiota in the pancreas of low

506   dose DSS-treated mice was dominated by the family Muribaculaceae (Figure 3E).

507   Notably, the 4 ASVs in Muribaculaceae, which were significantly enriched in the gut

508   by 0.2% DSS treatment (Figure 3A), also showed a trend of being enriched in the

509   pancreas of the low dose DSS-treated mice (Figure 3F). Other ASVs in the same family

510   showed no difference in pancreas between the low dose DSS-treated and control mice.

511   The bacterial load was not increased in the liver of the low dose DSS-treated mice

512   (Figure S11), suggesting that the gut microbiota specifically translocated to the

513   pancreas. Reduced production of cathelicidin-related antimicrobial peptide (CRAMP)

514   by pancreatic beta cells has been linked with the development of autoimmunity in the

515   pancreas and T1D [16]. We found that the expression of the *Cramp* gene in the pancreas

516   of 0.2% DSS-treated mice and FM_{DSS} mice was significantly lower than that in the

517   pancreas of their respective controls (Figure 3G). The reduced antimicrobial peptide

518   production may have allowed bacterial overgrowth in pancreas. Thus, the low dose DSS

519   enriched ASVs in the gut microbiota translocated to and overgrew in pancreas.

520   We then examined immune responses of pancreas to the bacterial translocation

521   and overgrowth. Infiltration of macrophages and total T cells were higher in the

522   pancreas of the low dose DSS-treated mice than control (Figure 3H). T cell

523   differentiation toward $CD4^+$ and $CD8^+$ T cells and T_H17 cells were also higher in low

524   dose DSS-treated mice than control, which may contribute to more inflammatory tissue

525   damage [47]. Moreover, the low dose DSS-treated mice had a decreased population of

526   regulatory T (T_{reg}) cells, which suppress the pathological immune response [48],

527   suggesting a continued inflammatory pancreatic milieu (Figure 3H). These immune

528   responses were also observed in FM_{DSS} mice but not in FM_{NC} mice (Figure S12).

529   ABX+DSS and ABX mice exhibited no detectable pancreatic bacterial loads via qPCR

530   and FISH and no differences in immune responses (Figure S13). Taken together, our

531   data supports the hypothesis that the downregulation of the pancreatic antimicrobial

532   peptide CRAMP may allow more bacteria to translocate from the gut to the pancreas

533   and overgrew there, which may lead to immune tolerance disruption and IDD

534   development.

535   **A pathobiont isolate from the family Muribaculaceae induced IDD in germfree**

536   **mice**

537   　Based on above findings, we hypothesized that specific bacteria represented by

538   the 4 ASVs in the family Muribaculaceae, which were enriched in both the gut and

539   pancreas, might represent the key mediators of low dose DSS-induced IDD. To further

540   examine the causal role of the bacteria in this family which were associated with low

541   dose DSS-induced IDD, we first aimed to obtain their pure cultures from fresh feces of

542   the low dose DSS-treated mice. Although bacteria in Muribaculaceae are dominant in

543   the mouse gut microbiota, they had not been cultured until recently [44]. After

544 sequence-guided screening of 13,079 colonies isolated using 46 different types of

545 media (Table S1), we obtained a pure culture (named strain MF 13079) and its finished

546 genomic sequence (Figure 4A and 4B). The genome of the strain MF 13079 had two

547 different 16S rRNA genes, each of which had 100% identity in the V3-V4 region with

548 ASV 6263 and ASV 6451 respectively (Figure S14). These two ASVs were members

549 of the family Muribaculaceae, which were among the 4 ASVs enriched in both the gut

550 and pancreas of low dose DSS-treated mice (Figure 3A). The nearest neighbor of MF

551 13079 in GenBank is *Duncaniella freteri* strain TLL-A3 but with only 93.7% homology

552 in 16S rRNA gene sequence (Figure 4C). The average nucleotide identity (ANI) values

553 between the genome of strain MF 13079 and all 10 publicly available genomes of

554 Muribaculaceae in GenBank ranged from 73.3% to 75.1%. Thus, MF 13079 may

555 represent a new genus in Muribaculaceae [49]. Moreover, we found the genes for

556 protecting against oxidative damage (COG0605 superoxide reductase, COG0753

557 catalase, COG0492 thioredoxin reductase, COG0450/COG2077/COG1225

558 peroxiredoxin) and genes for adhesion and immune evasion (COG0133/COG0159

559 tryptophan synthase) in the genome of MF 13079 (Table S2). Such genes may facilitate

560 the overgrowth of this gut bacterium in the pancreas and qualify it as a pathobiont [50].

561   To test if MF 13079 by itself can translocate from the gut to pancreas and induce

562 IDD, we inoculated only MF 13079 into germ-free adult C57BL/6 mice (Muri) by oral

563 gavage. A mouse-derived strain, *Akkermansia muciniphila* 139, was inoculated into

564 germ-free mice as control (Akk) [51]. Butyrate was not detected in either group (Figure

565 5A), and the pancreatic *Cramp* gene expression level showed a trend of being lower in

566 Muri group (Figure 5B). MF 13079 attained a significantly higher load in the pancreas

567 of Muri mice than *A. muciniphila* 139 in that of Akk mice (Figure 5C), suggesting that

568 the capacity of MF 13079 to translocate to the pancreas is much higher than that of *A.*

569 *muciniphila* 139. The Muri group, but not the Akk group, showed inflammation in the

570 pancreas and development of IDD (Figure 5D-5F). Thus, MF 13079 alone can

571 translocate from the gut to the pancreas, overgrew there and induce IDD.

572 To test whether MF 13079 can translocate from the gut to the pancreas and induce

573 IDD when in competition with a complex normal gut microbiota and in a host with

574 normal immunity, we transplanted cultured MF 13079 together with feces from control

575 mice by oral gavage into antibiotic-treated mice ($FM_{NC+Muri}$). Antibiotic-treated mice

576 inoculated with feces from control mice were denoted as FM_{NC}. We found that

577 $FM_{NC+Muri}$ mice had significantly lower cecum butyrate levels and pancreatic *Cramp*

578 expression than FM_{NC} mice (Figure 6A and 6B). We obtained the absolute abundance

579 of MF 13079 by multiplying the relative abundances of ASVs 6263 and 6451 with the

580 total bacterial load in the pancreas detected with qPCR of 16S rRNA genes. We found

581 that the load of MF 13079 in the pancreas of $FM_{NC+Muri}$ mice was

582 three orders of magnitude higher than that in the pancreas of FM_{NC} mice (Figure 6C).

583 Concomitantly, the $FM_{NC+Muri}$ mice showed an inflammatory pancreatic milieu and

584 increased blood glucose and decreased insulin in the OGTT (Figure 6D-6F). Thus,

585   when transplanted together with the fecal microbiota from healthy mice, MF 13079 still

586   translocated to pancreas and induced IDD in antibiotic-treated mice.

587   As recipient mice had normal gut barrier function, we tested other possible routes

588   for translocation of gut pathobionts to pancreas. Notably, MF 13079 has a complete

589   flagellar assembly pathway in its genome based on KEGG database querying, and a

590   flagellar structure was observed with scanning electron microscopy (Figure 4A, Figure

591   S15 and Table S2). We tested bacterial motility by an agar-based motility assay, and

592   MF 13079 demonstrated notable motility in vitro (Figure S15). It provides a means by

593   which MF 13079 might translocate from the gut to the pancreas via the pancreatic duct.

594   Interestingly, we also detected a much higher load of MF 13079 in the mesenteric

595   lymph nodes of Muri mice than *A. muciniphila* 139 in those of Akk mice (Figure S16),

596   which might represent another pathway for MF 13079 to gain access to the pancreas

597   via lymphatic drainage routes [52, 53].

Discussion

599   Our study demonstrated that novel pathobionts enriched in a low DSS-disrupted

600   gut microbiota can translocate to pancreas and induce IDD in mice. Such pathobionts

601   are both necessary and sufficient to induce IDD. Genetic predisposition to IDD here

602   was not required from the host side as the mice we used were with no known relevant

603   genetic defects. More importantly, a single pathobiont MF 13079 isolated from the

604   family Muribaculaceae was sufficient to induce IDD when mono-associated with

605 wildtype germfree mice. The fact that IDD was induced when MF 13079 was mixed

606 with normal gut microbiota and transplanted to antibiotic treated wildtype mice which

607 have well-developed immune system shows that predominant population level of this

608 pathobiont in the gut is sufficient to IDD development. Thus, this pathobiont has been

609 identified as an etiological factor for inducing IDD as what we did fulfilled Koch's

610 postulates which were established for identifying the causal agent for an infectious

611 disease. This IDD-inducing capacity may be a redundant function of many gut

612 pathobionts in the same mouse, however, translocation of one such pathobiont to

613 pancreas seems to be enough for inducing IDD and host genetic defect is not required.

614   Studies in humans have shown that acute or chronic inflammation of the entire

615 pancreas may drive beta-cell death and lead to IDD [54]. Previous studies showed that

616 decreased gene expression of pancreatic CRAMP stimulated the inflammatory

617 activities of intrapancreatic immune cells and led to destruction of beta cells [16]. Our

618 study showed that enrichment and overgrowth of pathobionts in the pancreas is

619 necessary for CRAMP-induced stimulation of local immune cells because antibiotic

620 removal of the gut microbiota resulted in pancreatic microbiome depletion and

621 abolished DSS-induced IDD.

622   Studies showed that reduced butyrate production in the gut may drive the

623 decreased gene expression of pancreatic CRAMP [?]. This might be a mechanism for

624 induction of pancreatic inflammation and IDD in our low DSS model. The low dose

625 DSS treated mice had depletion of butyrate producers and reduced butyrate

626 production in their gut and decreased gene expression of pancreatic CRAMP. This

627 warrants further studies.

628 Conclusion

629   Our study shows that toxic chemicals such as DSS may disrupt the gut microbiota

630 and lead to serious health consequences even at a low dosage which does not cause

631 acute local responses in the gut. The overgrowth in the gut and translocation to the

632 pancreas of pathobionts may induce inflammation in the pancreas, destruct beta cells

633 and lead to IDD. This study inspires us to search for similar pathobionts in patients with

634 IDD. Suppression of the overgrowth of pathobionts in the gut and prevention of their

635 translocation to the pancreas via restoration of a normal structure of the gut microbiota

636 may become a promising ecological approach for managing IDD.

637 List of abbreviation

638 **IDD**: Insulin-dependent diabetes; **T1D**: type 1 diabetes; **SCFAs**: short-chain fatty acids;

639 **DSS**: dextran sulfate sodium; **OGTT**: oral glucose tolerance test; **ITT**: insulin tolerance

640 test; **PCoA**: principal coordinate analysis; **ASVs**: amplicon sequence variants;

641 **PERMANOVA**: permutational multivariate analysis of variance; **sPLS-DA**: sparse

642 partial least squares discriminant analysis; **FISH**: fluorescence in situ hybridization;

643 **CRAMP**: cathelicidin-related antimicrobial peptide

644 Declarations

645 *Ethics approval and consent to participate*

646   All experimental procedures for specific pathogen free (SPF) mice were approved by

647   the Institutional Animal Care and Use Committee (IACUC) of the School of Life

648   Sciences and Biotechnology of Shanghai Jiao Tong University (no. 2014005). The

649   procedures for the germ-free mice experiments were approved by the Institutional

650   Animal Care and Use Committee of SLAC Inc (no. 20190201001).

651   ***Consent for publication***

652   Not applicable

653   ***Availability of data and materials***

654   The data that support the findings of this study are available from the corresponding

655   author upon request. The 16S rRNA gene sequences of Muribaculaceae strain

656   MF13079 has been submitted to the GenBank with the accession No. MT921595 and

657   MT921596. The whole-genome sequence of Muribaculaceae strain MF13079 has been

658   submitted to the NCBI under accession No. PRJNA576346.The raw Illumine sequence

659   data generated in this study are available in the sequence read archive (SRA) at NCBI

660   under accession No. SRP278697.

661   ***Competing interests***

662   The authors declare no competing interests.

663   ***Founding***

667   ***Acknowledgements***

668 Not applicable

669 *Author's contributions*

670 C. Z. and L. Z. conceived, planned and supervised this study. X. Y. carried out the

671 animal experiments and most experiments in lab. X. X. and Z. R. isolated the

672 *Akkermansia muciniphila* strain 139 and provided the protocol of *A. muciniphila* strain

673 139 related animal experiment. X. Y. and J. N. performed the flow cytometry evaluation

674 of subtypes of leukocytes in the pancreas. G. W. and Z. W. provided help of genome

675 sequencing data analysis. C. Z. and X. Y. analyzed the data and generated the figures

676 and tables. C. Z., L. Z., H. Y., J. Y., X. Y. and G. W. prepared the manuscript. All

677 authors approved the manuscript.

678

679 **References**

680 1.   Petersmann A, Muller-Wieland D, Muller UA, Landgraf R, Nauck M,
681   Freckmann G, Heinemann L, Schleicher E: **Definition, Classification and**
682   **Diagnosis of Diabetes Mellitus**. *Exp Clin Endocrinol Diabetes* 2019, **127**(S
683   01):S1-S7.
684 2.   Beck RW, Bergenstal RM, Laffel LM, Pickup JC: **Advances in technology**
685   **for management of type 1 diabetes**. *Lancet* 2019, **394**(10205):1265-1273.
686 3.   Stamatouli AM, Quandt Z, Perdigoto AL, Clark PL, Kluger H, Weiss SA,
687   Gettinger S, Sznol M, Young A, Rushakoff R *et al*: **Collateral Damage:**
688   **Insulin-Dependent Diabetes Induced With Checkpoint Inhibitors**.
689   *Diabetes* 2018, **67**(8):1471-1480.
690 4.   Dahlquist GG, Blom LG, Persson LA, Sandstrom AI, Wall SG: **Dietary**
691   **factors and the risk of developing insulin dependent diabetes in**
692   **childhood**. *BMJ* 1990, **300**(6735):1302-1306.
693 5.   Chee YJ, Ng SJH, Yeoh E: **Diabetic ketoacidosis precipitated by Covid-19**
694   **in a patient with newly diagnosed diabetes mellitus**. *Diabetes Res Clin*
695   *Pract* 2020, **164**:108166.
696 6.   Rewers M, Ludvigsson J: **Environmental risk factors for type 1 diabetes**.
697   *Lancet* 2016, **387**(10035):2340-2348.
698 7.   Costa FR, Francozo MC, de Oliveira GG, Ignacio A, Castoldi A, Zamboni DS,
699   Ramos SG, Camara NO, de Zoete MR, Palm NW *et al*: **Gut microbiota**
700   **translocation to the pancreatic lymph nodes triggers NOD2 activation and**
701   **contributes to T1D onset**. *J Exp Med* 2016, **213**(7):1223-1239.

702 8. Vatanen T, Franzosa EA, Schwager R, Tripathi S, Arthur TD, Vehik K,
703   Lernmark A, Hagopian WA, Rewers MJ, She JX *et al*: **The human gut**
704   **microbiome in early-onset type 1 diabetes from the TEDDY study**. *Nature*
705   2018, **562**(7728):589-594.

706 9. Vehik K, Lynch KF, Wong MC, Tian X, Ross MC, Gibbs RA, Ajami NJ,
707   Petrosino JF, Rewers M, Toppari J *et al*: **Prospective virome analyses in**
708   **young children at increased genetic risk for type 1 diabetes**. *Nat Med* 2019,
709   **25**(12):1865-1872.

710 10. Antvorskov JC, Halldorsson TI, Josefsen K, Svensson J, Granstrom C, Roep
711   BO, Olesen TH, Hrolfsdottir L, Buschard K, Olsen SF: **Association between**
712   **maternal gluten intake and type 1 diabetes in offspring: national**
713   **prospective cohort study in Denmark**. *BMJ* 2018, **362**:k3547.

714 11. Wen L, Ley RE, Volchkov PY, Stranges PB, Avanesyan L, Stonebraker AC,
715   Hu C, Wong FS, Szot GL, Bluestone JA *et al*: **Innate immunity and**
716   **intestinal microbiota in the development of Type 1 diabetes**. *Nature* 2008,
717   **455**(7216):1109-1113.

718 12. Burrows MP, Volchkov P, Kobayashi KS, Chervonsky AV: **Microbiota**
719   **regulates type 1 diabetes through Toll-like receptors**. *Proc Natl Acad Sci U*
720   *S A* 2015, **112**(32):9973-9977.

721 13. Markle JG, Frank DN, Mortin-Toth S, Robertson CE, Feazel LM, Rolle-
722   Kampczyk U, von Bergen M, McCoy KD, Macpherson AJ, Danska JS: **Sex**
723   **differences in the gut microbiome drive hormone-dependent regulation of**
724   **autoimmunity**. *Science* 2013, **339**(6123):1084-1088.

725 14. Candon S, Perez-Arroyo A, Marquet C, Valette F, Foray AP, Pelletier B,
726   Milani C, Ventura M, Bach JF, Chatenoud L: **Antibiotics in early life alter**
727   **the gut microbiome and increase disease incidence in a spontaneous**
728   **mouse model of autoimmune insulin-dependent diabetes**. *PLoS One* 2015,
729   **10**(5):e0125448.

730 15. Livanos AE, Greiner TU, Vangay P, Pathmasiri W, Stewart D, McRitchie S,
731   Li H, Chung J, Sohn J, Kim S *et al*: **Antibiotic-mediated gut microbiome**
732   **perturbation accelerates development of type 1 diabetes in mice**. *Nat*
733   *Microbiol* 2016, **1**(11):16140.

734 16. Sun J, Furio L, Mecheri R, van der Does AM, Lundeberg E, Saveanu L, Chen
735   Y, van Endert P, Agerberth B, Diana J: **Pancreatic beta-Cells Limit**
736   **Autoimmune Diabetes via an Immunoregulatory Antimicrobial Peptide**
737   **Expressed under the Influence of the Gut Microbiota**. *Immunity* 2015,
738   **43**(2):304-317.

739 17. Wu QL, Chen TT, El-Nezami H, Savidge TC: **Food ingredients in human**
740   **health: Ecological and metabolic perspectives implicating gut microbiota**
741   **function**. *Trends Food Sci Tech* 2020, **100**:103-117.

18. Chassaing B, Srinivasan G, Delgado MA, Young AN, Gewirtz AT, Vijay-Kumar M: **Fecal lipocalin 2, a sensitive and broadly dynamic non-invasive biomarker for intestinal inflammation**. *PLoS One* 2012, **7**(9):e44328.

19. Okamoto T, Sasaki M, Tsujikawa T, Fujiyama Y, Bamba T, Kusunoki M: **Preventive efficacy of butyrate enemas and oral administration of Clostridium butyricum M588 in dextran sodium sulfate-induced colitis in rats**. *J Gastroenterol* 2000, **35**(5):341-346.

20. Zhang Q, Wu Y, Wang J, Wu G, Long W, Xue Z, Wang L, Zhang X, Pang X, Zhao Y *et al*: **Accelerated dysbiosis of gut microbiota during aggravation of DSS-induced colitis by a butyrate-producing bacterium**. *Sci Rep* 2016, **6**:27572.

21. Zhao L, Zhang F, Ding X, Wu G, Lam YY, Wang X, Fu H, Xue X, Lu C, Ma J *et al*: **Gut bacteria selectively promoted by dietary fibers alleviate type 2 diabetes**. *Science* 2018, **359**(6380):1151-1156.

22. Rakoff-Nahoum S, Paglino J, Eslami-Varzaneh F, Edberg S, Medzhitov R: **Recognition of commensal microflora by toll-like receptors is required for intestinal homeostasis**. *Cell* 2004, **118**(2):229-241.

23. Zhang C, Yin A, Li H, Wang R, Wu G, Shen J, Zhang M, Wang L, Hou Y, Ouyang H *et al*: **Dietary Modulation of Gut Microbiota Contributes to Alleviation of Both Genetic and Simple Obesity in Children**. *EBioMedicine* 2015, **2**(8):968-984.

24. Plovier H, Everard A, Druart C, Depommier C, Van Hul M, Geurts L, Chilloux J, Ottman N, Duparc T, Lichtenstein L *et al*: **A purified membrane protein from Akkermansia muciniphila or the pasteurized bacterium improves metabolism in obese and diabetic mice**. *Nat Med* 2017, **23**(1):107-113.

25. Zaki MH, Boyd KL, Vogel P, Kastan MB, Lamkanfi M, Kanneganti TD: **The NLRP3 inflammasome protects against loss of epithelial integrity and mortality during experimental colitis**. *Immunity* 2010, **32**(3):379-391.

26. Roch AM, Maatman TK, Cook TG, Wu HH, Merfeld-Clauss S, Traktuev DO, March KL, Zyromski NJ: **Therapeutic Use of Adipose-Derived Stromal Cells in a Murine Model of Acute Pancreatitis**. *J Gastrointest Surg* 2020, **24**(1):67-75.

27. Wang CJ, Zhou ZG, Holmqvist A, Zhang H, Li Y, Adell G, Sun XF: **Survivin expression quantified by Image Pro-Plus compared with visual assessment**. *Appl Immunohistochem Mol Morphol* 2009, **17**(6):530-535.

28. Zou Y, Xue W, Luo G, Deng Z, Qin P, Guo R, Sun H, Xia Y, Liang S, Dai Y *et al*: **1,520 reference genomes from cultivated human gut bacteria enable functional microbiome analyses**. *Nat Biotechnol* 2019, **37**(2):179-185.

29. Chin CS, Alexander DH, Marks P, Klammer AA, Drake J, Heiner C, Clum A, Copeland A, Huddleston J, Eichler EE *et al*: **Nonhybrid, finished microbial**

genome assemblies from long-read SMRT sequencing data. *Nat Methods* 2013, **10**(6):563-569.

30. Seemann T: **Prokka: rapid prokaryotic genome annotation**. *Bioinformatics* 2014, **30**(14):2068-2069.

31. Nadkarni MA, Martin FE, Jacques NA, Hunter N: **Determination of bacterial load by real-time PCR using a broad-range (universal) probe and primers set**. *Microbiology (Reading)* 2002, **148**(Pt 1):257-266.

32. Sunde PT, Olsen I, Gobel UB, Theegarten D, Winter S, Debelian GJ, Tronstad L, Moter A: **Fluorescence in situ hybridization (FISH) for direct visualization of bacteria in periapical lesions of asymptomatic root-filled teeth**. *Microbiology (Reading)* 2003, **149**(Pt 5):1095-1102.

33. Thimm T, Tebbe CC: **Protocol for rapid fluorescence in situ hybridization of bacteria in cryosections of microarthropods**. *Appl Environ Microbiol* 2003, **69**(5):2875-2878.

34. Choi YS, Kim YC, Baek KJ, Choi Y: **In Situ Detection of Bacteria within Paraffin-embedded Tissues Using a Digoxin-labeled DNA Probe Targeting 16S rRNA**. *J Vis Exp* 2015(99):e52836.

35. Callahan BJ, McMurdie PJ, Rosen MJ, Han AW, Johnson AJ, Holmes SP: **DADA2: High-resolution sample inference from Illumina amplicon data**. *Nat Methods* 2016, **13**(7):581-583.

36. Davis NM, Proctor DM, Holmes SP, Relman DA, Callahan BJ: **Simple statistical identification and removal of contaminant sequences in marker-gene and metagenomics data**. *Microbiome* 2018, **6**(1):226.

37. Godon JJ, Zumstein E, Dabert P, Habouzit F, Moletta R: **Molecular microbial diversity of an anaerobic digestor as determined by small-subunit rDNA sequence analysis**. *Appl Environ Microbiol* 1997, **63**(7):2802-2813.

38. Quast C, Pruesse E, Yilmaz P, Gerken J, Schweer T, Yarza P, Peplies J, Glockner FO: **The SILVA ribosomal RNA gene database project: improved data processing and web-based tools**. *Nucleic Acids Res* 2013, **41**(Database issue):D590-596.

39. Anderson MJ: **A new method for non-parametric multivariate analysis of variance**. *Austral Ecol* 2001, **26**(1):32-46.

40. Le Cao KA, Boitard S, Besse P: **Sparse PLS discriminant analysis: biologically relevant feature selection and graphical displays for multiclass problems**. *BMC Bioinformatics* 2011, **12**:253.

41. Rohart F, Gautier B, Singh A, Le Cao KA: **mixOmics: An R package for 'omics feature selection and multiple data integration**. *PLoS Comput Biol* 2017, **13**(11):e1005752.

42. Sorini C, Cosorich I, Lo Conte M, De Giorgi L, Facciotti F, Luciano R, Rocchi M, Ferrarese R, Sanvito F, Canducci F *et al*: **Loss of gut barrier**

824 **integrity triggers activation of islet-reactive T cells and autoimmune**
825 **diabetes**. *Proc Natl Acad Sci U S A* 2019, **116**(30):15140-15149.

826 43. Lundberg R, Toft MF, August B, Hansen AK, Hansen CH: **Antibiotic-treated**
827 **versus germ-free rodents for microbiota transplantation studies**. *Gut*
828 *Microbes* 2016, **7**(1):68-74.

829 44. Lagkouvardos I, Lesker TR, Hitch TCA, Galvez EJC, Smit N, Neuhaus K,
830 Wang J, Baines JF, Abt B, Stecher B *et al*: **Sequence and cultivation study**
831 **of Muribaculaceae reveals novel species, host preference, and functional**
832 **potential of this yet undescribed family**. *Microbiome* 2019, **7**(1):28.

833 45. Chen J, Vitetta L: **The Role of Butyrate in Attenuating Pathobiont-Induced**
834 **Hyperinflammation**. *Immune Netw* 2020, **20**(2):e15.

835 46. Thomas RM, Jobin C: **Microbiota in pancreatic health and disease: the**
836 **next frontier in microbiome research**. *Nat Rev Gastroenterol Hepatol* 2020,
837 **17**(1):53-64.

838 47. Torchinsky MB, Garaude J, Martin AP, Blander JM: **Innate immune**
839 **recognition of infected apoptotic cells directs T(H)17 cell differentiation**.
840 *Nature* 2009, **458**(7234):78-82.

841 48. Cebula A, Seweryn M, Rempala GA, Pabla SS, McIndoe RA, Denning TL,
842 Bry L, Kraj P, Kisielow P, Ignatowicz L: **Thymus-derived regulatory T cells**
843 **contribute to tolerance to commensal microbiota**. *Nature* 2013,
844 **497**(7448):258-262.

845 49. Tindall BJ, Rossello-Mora R, Busse HJ, Ludwig W, Kampfer P: **Notes on the**
846 **characterization of prokaryote strains for taxonomic purposes**. *Int J Syst*
847 *Evol Microbiol* 2010, **60**(Pt 1):249-266.

848 50. Ha CWY, Martin A, Sepich-Poore GD, Shi B, Wang Y, Gouin K, Humphrey
849 G, Sanders K, Ratnayake Y, Chan KSL *et al*: **Translocation of Viable Gut**
850 **Microbiota to Mesenteric Adipose Drives Formation of Creeping Fat in**
851 **Humans**. *Cell* 2020, **183**(3):666-683 e617.

852 51. Zhai R, Xue X, Zhang L, Yang X, Zhao L, Zhang C: **Strain-Specific Anti-**
853 **inflammatory Properties of Two Akkermansia muciniphila Strains on**
854 **Chronic Colitis in Mice**. *Front Cell Infect Microbiol* 2019, **9**:239.

855 52. Diehl GE, Longman RS, Zhang JX, Breart B, Galan C, Cuesta A, Schwab SR,
856 Littman DR: **Microbiota restricts trafficking of bacteria to mesenteric**
857 **lymph nodes by CX(3)CR1(hi) cells**. *Nature* 2013, **494**(7435):116-120.

858 53. Bravo-Blas A, Utriainen L, Clay SL, Kastele V, Cerovic V, Cunningham AF,
859 Henderson IR, Wall DM, Milling SWF: **Salmonella enterica Serovar**
860 **Typhimurium Travels to Mesenteric Lymph Nodes Both with Host Cells**
861 **and Autonomously**. *J Immunol* 2019, **202**(1):260-267.

862 54. Vecchio F, Messina G, Giovenzana A, Petrelli A: **New Evidence of Exocrine**
863 **Pancreatopathy in Pre-symptomatic and Symptomatic Type 1 Diabetes**.
864 *Curr Diab Rep* 2019, **19**(10):92.
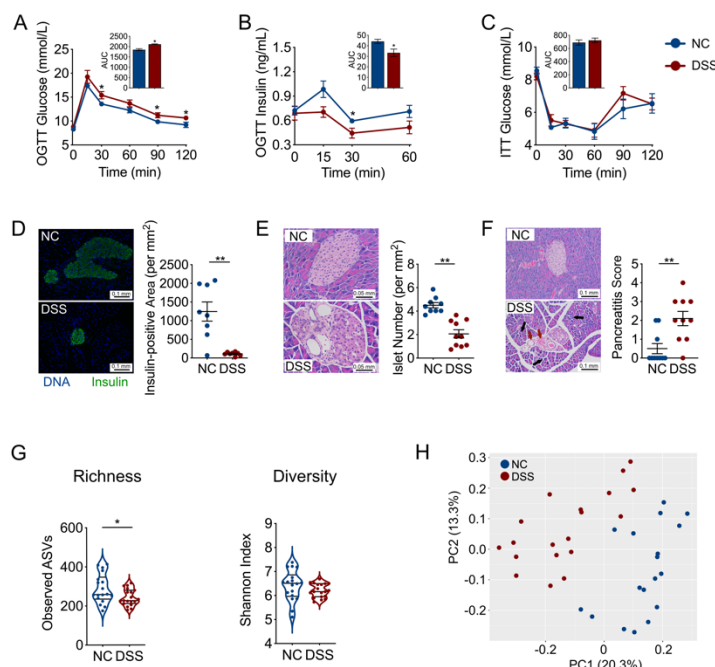
865

866 **Figure**

867 **Figure 1**

868

Figure 1 | IDD induced by 0.2% DSS treatment in mice (A) Blood glucose and **(B)** insulin levels of normal control (NC) and DSS-treated mice, as measured by an oral glucose tolerance test (OGTT) (the area under the curve (AUC) is shown in the inset panels). NC group, n=9; DSS group, n=7. **(C)** Blood glucose levels of NC and DSS-treated mice as measured by an insulin tolerance test (ITT) (the AUC is shown in the inset panels). NC group, n=8; DSS group, n=9. **(D)** Histological sections of pancreatic tissue (200×, scale bar = 0.1 mm) from NC and DSS-treated mice stained for insulin (green) and DNA (blue), and the insulin-positive area was quantified (at right). NC group, n=8; DSS group, n=8. **(E)** The number of islets per mm^2 of pancreatic tissue was calculated based on H&E-stained histological sections of pancreatic tissue (400×, scale bar = 0.05 mm) from NC and DSS-treated mice. NC group, n=9; DSS group, n=10. **(F)** The histologic pancreatitis score was evaluated by edema, inflammation, and vacuolization in the H&E-stained histological sections of pancreatic tissue (200×, scale bar = 0.1 mm) from NC and DSS-treated mice. Black arrows, scattered structure; Red arrows, increased peri-islet neovascularization. NC group, n=10; DSS group, n=10. **(G)** The alpha-diversity of gut microbiota in NC and DSS-treated mice. **(H)** Overall gut microbial structure in NC and DSS-treated mice. Principal coordinate analysis (PCoA) was performed on the basis of Bray-Curtis distance at the amplicon sequence variant (ASV) level. For **(G)** and **(H)**, NC group, n=17; DSS group, n=18. The data in **(A)-(F)** are shown as the mean ± SEM, and Student's t-test (two-tailed) was used to analyze difference between NC and DSS groups. *P <0.05 and **P <0.01. NC, control mice provided pure drinking water; DSS, mice treated with 0.2% (w/v) DSS in drinking water.
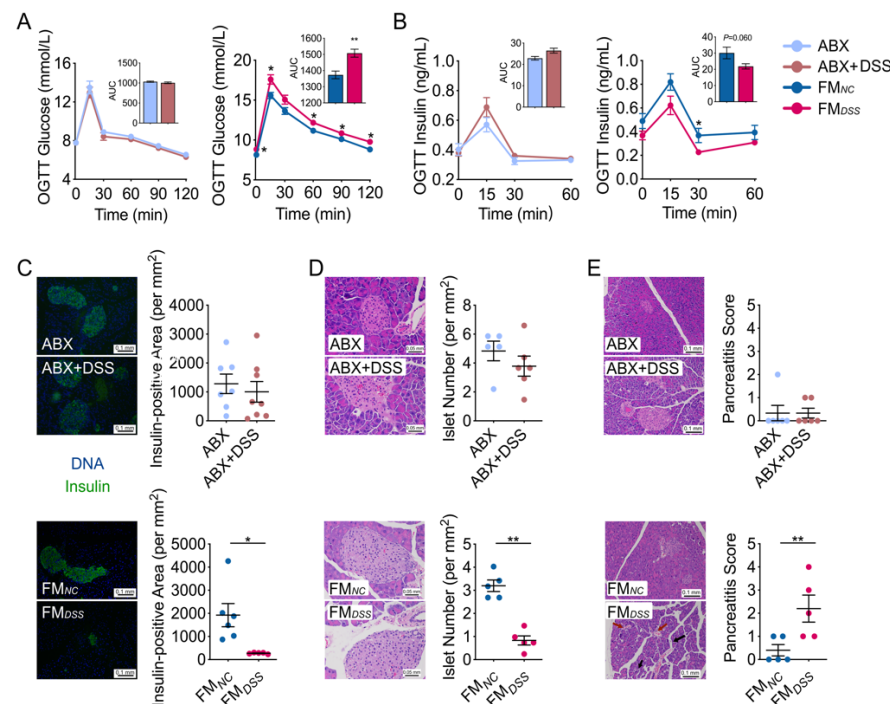
889

Figure 2

Figure 2 | The gut microbiota disrupted by 0.2% DSS was both necessary and sufficient for inducing IDD. (A) Blood glucose and **(B)** insulin levels with the AUC in the OGTT of ABX, ABX+DSS, FM_{DSS} and FM_{NC} mice. For **(A)**, ABX group, n=10; ABX+DSS group, n=8; FM_{NC} group, n=8; FM_{DSS} group, n=8. For **(B)**, ABX group, n=9; ABX+DSS group, n=7; FM_{NC} group, n=6; FM_{DSS} group, n=6. **(C)** Histological sections of pancreatic tissue (200×, scale bar = 0.1 mm) from ABX, ABX+DSS, FM_{DSS} and FM_{NC} mice stained for insulin (green) and DNA (blue), and the insulin-positive area was quantified (at bottom). ABX group, n=7; ABX+DSS group, n=8; FM_{NC} group, n=6; FM_{DSS} group, n=5. **(D)** The number of islets per mm^2 of pancreatic tissue was calculated based on H&E-stained histological sections of pancreatic tissue (400×, scale bar = 0.05 mm) from ABX, ABX+DSS, FM_{DSS} and FM_{NC} mice. ABX group, n=5; ABX+DSS group, n=6; FM_{NC} group, n=5; FM_{DSS} group, n=5. **(E)** The histologic pancreatitis score was evaluated by edema, inflammation, and vacuolization in H&E-stained histological sections of pancreatic tissue (200×, scale bar = 0.1 mm) from ABX, ABX+DSS, FM_{DSS} and FM_{NC} mice. Black arrows, scattered structure; Red arrows, increased peri-islet neovascularization. ABX group, n=6; ABX+DSS group, n=6; FM_{NC} group, n=5; FM_{DSS} group, n=5. The data in **(A)-(E)** are shown as the mean ± SEM, and Student's t-test (two-tailed) was used to analyze the following pairs of groups: ABX vs. ABX+DSS, or FM_{NC} vs. FM_{DSS}. *P <0.05 and **P <0.01. ABX, antibiotic cocktail-treated mice provided pure water; ABX+DSS, antibiotic cocktail-treated mice treated with 0.2% (w/v) DSS added to drinking water; FM_{NC}, antibiotic cocktail-treated mice inoculated with the fecal microbiota from mice in the NC group and provided pure water; FM_{DSS}, antibiotic cocktail-treated mice inoculated with the fecal microbiota from mice in the DSS group and provided pure water.

914 **Figure 3**

915

916 **Figure 3 | An increase in bacterial load and the impairment of immune tolerance in the**
917 **pancreas. (A)** Thirty ASVs that were significantly altered after 3 months of 0.2% DSS treatment,
918 as identified using sPLS-DA models. The cluster tree on the left shows associations between these
919 ASVs, as determined by the Spearman correlation coefficient based on their relative abundances
920 among all the samples. The heat map shows the relative abundance ($\log_{10}$ transformed) of each ASV
921 in a sample from an individual mouse. NC group, n=17; DSS group, n=18. **(B)** The butyrate content
922 in the cecum of mice. NC, n=8; DSS, n=9; FM_{NC} n=8; FM_{DSS}, n=8. The bacterial load in the pancreas
923 as measured by **(C)** real-time qPCR and **(D)** fluorescence in situ hybridization (FISH) of 16S rRNA.
924 NC, n=8; DSS, n=9; FM_{NC}, n=5; FM_{DSS}, n=5. **(E)** Distribution of family-level phylotypes in the

925   pancreas of NC and DSS-treated mice. The names of the top 10 most abundant families in the DSS

926   group are shown. The abundance was determined by the relative abundances of these families with

927   the total bacterial load in the pancreas detected with qPCR of 16S rRNA genes. NC, n=9; DSS, n=8.

928   **(F)** The load of the 4 Muribaculaceae ASVs in the pancreas. The load was determined by

929   multiplying the relative abundances of these ASVs with the total bacterial load in the pancreas

930   detected with qPCR of 16S rRNA genes. NC, n=9; DSS, n=8. **(G)** *Cramp* expression in the pancreas

931   of mice. NC, n=10; DSS, n=10; ABX, n=6; ABX+DSS, n=6; FM_{NC}, n=5; FM_{DSS}, n=5. **(H)** Flow

932   cytometry evaluation of leukocyte subtypes in the pancreas of NC and DSS-treated mice. Data are

933   presented as the frequency of gated cells (from left to right: F4/80$^+$ macrophages, CD3$^+$ cells, CD8$^+$

934   T cells, CD8$^+$ IFNγ$^+$ cells, CD4$^+$ T cells, IL-17A$^+$ CD4$^+$ cells, and Foxp3$^+$ CD4$^+$ cells) among the

935   CD45$^+$ population of cells per mouse. NC group, n=4-5; DSS group, n=4-5. The data are shown as

936   the mean ± SEM, and Student's t-test (two-tailed) was used to analyze differences between the NC

937   and DSS groups or the FM_{NC} and FM_{DSS} groups. *$P <0.05$ and **$P <0.01$.

938

939

940

941

942

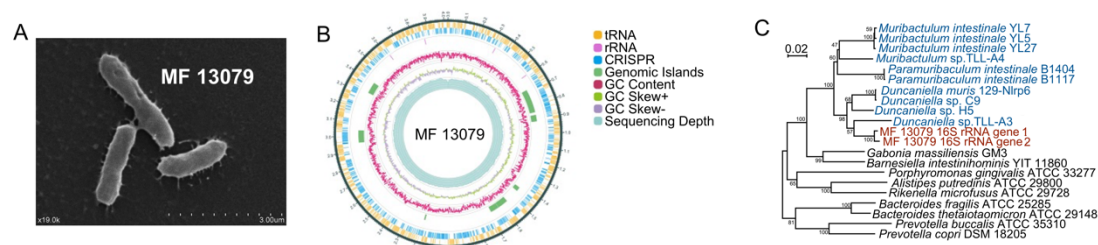943

944

945

946   **Figure 4**

947

948   **Figure 4 | A gut-derived Muribaculaceae isolate enriched by 0.2% DSS treatment (A)** A

949   scanning electron microscopy image of a pure isolate from the Muribaculaceae family (named strain

950   MF 13079) that was enriched in the gut of DSS-treated mice. **(B)** Genome atlas of the MF13079

951   strain of Muribaculaceae. From outer to inner: circle 1. tRNAs; circle 2. rRNAs; circle 3. CRISPR

952   sites; circle 4. mean centered GC content; circle 5. Sequencing depth. **(C)** A phylogenetic tree

953   constructed with the 16 rRNA gene of MF 13079 (red), other Muribaculaceae bacteria (blue) and

954   typical bacterial strains in Bacteroidetes.

955
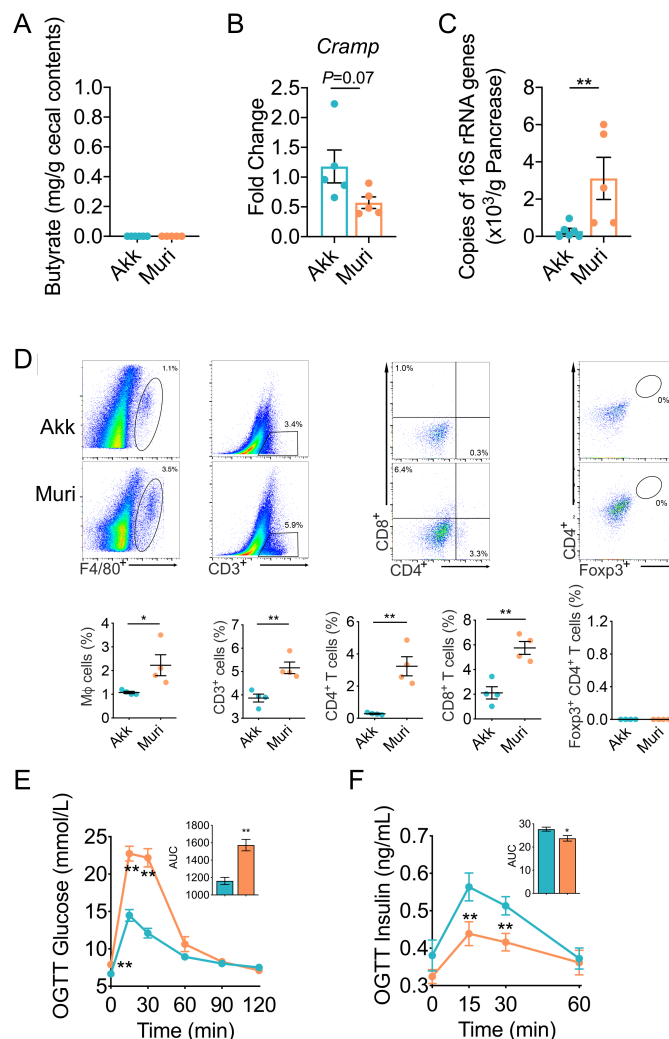
956 **Figure 5**

957

958 **Figure 5 | MF13079 induced IDD by translocating to the pancreas in germ-free mice. (A)** The

959 butyrate content in the cecum of mice in the Muri and Akk groups. Akk, n=12; Muri, n=11. **(B)** *Cramp*

960 expression in the pancreas of mice in the Muri and Akk groups. Akk, n=6; Muri, n=5. **(C)** The MF

961 13079 load in the pancreas of mice in the Muri and Akk groups assessed via qPCR of the 16S rRNA

962 gene of each strain. Akk, n=6; Muri, n=5. **(D)** Flow cytometry evaluation of leukocyte subtypes in the

963 pancreas of mice in the Muri and Akk groups. Data are presented as the frequency of gated cells (left to

964 right: F4/80^{+} macrophages, CD3^{+} cells, CD8^{+} T cells, CD4^{+} T cells, and Foxp3^{+} CD4^{+} cells) among the

965 CD45^{+} population of cells per mouse. Akk, n=5; Muri, n=5. Blood glucose **(E)** and insulin **(F)** levels of

966 the mice in Muri and Akk groups as measured by OGTT (the AUC is shown in the inset graph). For

967 **(E)**, Akk, n=12; Muri, n=11. For **(F)**, Akk, n=10; Muri, n=10. Muri, germ-free mice inoculated with

968 the MF 13079 strain and provided pure water; Akk, germ-free mice inoculated with the *Akkermansia*

969 *muciniphila* strain 139 and provided pure water. In **(A)-(F)**, the data are shown as the mean ± SEM,

970 and Student's t-test (two-tailed) was used to analyze the differences between the Muri and Akk groups.

971 *P <0.05 and **P <0.01.

972
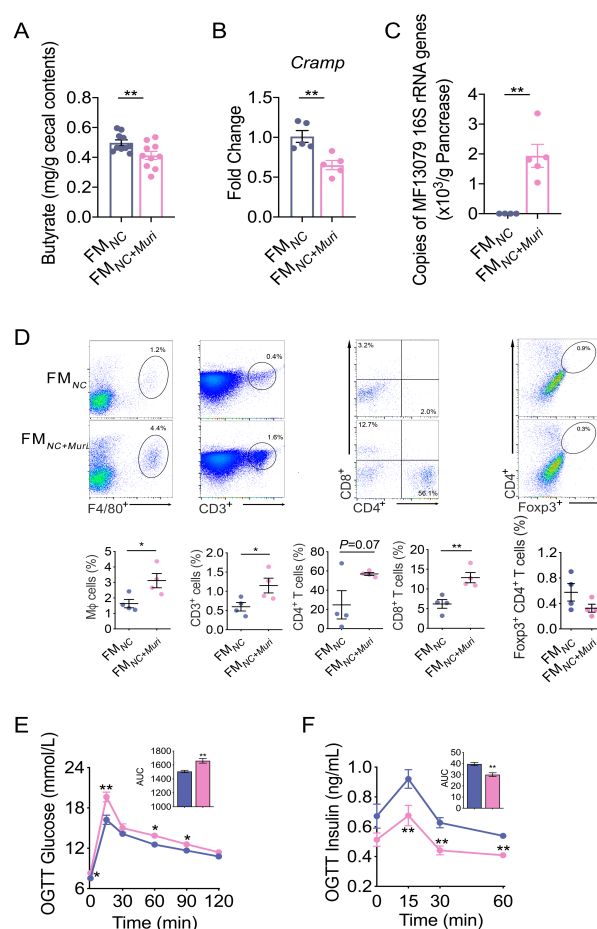
Figure 6

Figure 6 | MF 13079 translocated from the gut to the pancreas and induce IDD when in competition with a complex gut microbiota. (A) The butyrate content in the cecum of FM_{NC} and $FM_{NC+Muri}$ mice. FM_{NC}, n=10; $FM_{NC+Muri}$, n=10. **(B)** *Cramp* expression in the pancreas of FM_{NC} and $FM_{NC+Muri}$ mice. FM_{NC}, n=5; $FM_{NC+Muri}$, n=5. **(C)** The amount of the MF 13079 in the pancreas of $FM_{NC+Muri}$ and FM_{NC} mice assessed with the method described in Figure 3F. FM_{NC}, n=4; $FM_{NC+Muri}$, n=5. **(D)** Flow cytometry evaluation of leukocyte subtypes in the pancreas of $FM_{NC+Muri}$ and FM_{NC} mice. Data are presented as the frequency of gated cells (left to right: F4/80+ macrophages, CD3+ cells, CD8+ T cells, CD4+ T cells, and Foxp3+ CD4+ cells) among the CD45+ population of cells per mouse. FM_{NC}, n=4; $FM_{NC+Muri}$, n=4. Blood glucose **(E)** and insulin **(F)** levels of $FM_{NC+Muri}$ and FM_{NC} mice as measured by an OGTT (the AUC is shown in the inset graph). For **(E)**, FM_{NC}, n=10; $FM_{NC+Muri}$, n=10. For **(F)**, FM_{NC}, n=8; $FM_{NC+Muri}$, n=10. FM_{DSS}, antibiotic cocktail-treated mice inoculated with the fecal microbiota from mice in the DSS group and provided pure water; $FM_{NC+Muri}$, antibiotic cocktail-treated mice inoculated with a mixture of the fecal microbiota of the NC group and the MF 13079 strain and provided pure water. In **(A)-(F)**, the data are shown as the mean ± SEM, and Student's t-test (two-tailed) was used to analyze the differences between the FM_{NC} and $FM_{NC+Muri}$ groups. *P <0.05 and **P <0.01.

991 **Supplementary Files**

992 1. File name: Supplementary Figures

993 File Format: PDF

994 Discerption: Supplementary Figure S1 to S16

995 Fig. S1| Fasting C-Peptide in the mice with and without 0.2% DSS.

996 Fig. S2| Serum amylase (AMS) and serum lipase levels in each group.

997 Fig. S3| 0.2% DSS increased food and water intake but did not change energy intake of mice.

998 Fig. S4| 0.2% DSS did not change the lipid accumulation in mice.

999 Fig. S5| 0.2% DSS did not impair gut barrier integrity and induce inflammation.

1000 Fig. S6| The gut microbiota had been depleted by more than 99% in the mice with a cocktail of

1001 antibiotics for 5 weeks.

1002 Fig. S7| The recipient mice developed a gut microbiota more similar to their donor mice.

1003 Fig. S8| Optimal classification performance of the sPLS-DA model of the gut microbial

1004 structure in NC and DSS mice.

1005 Fig. S9| Fluorescence in situ hybridization (FISH) of 16S rRNA in the pancreas of antibiotic

1006 treated mice.

1007 Fig. S10| Fluorescence in situ hybridization (FISH) of 16S rRNA in the pancreas in fecal

1008 microbiota transplanted mice.

1009 Fig. S11| The bacterial load in the liver as measured by real-time qPCR of 16S rRNA gene.

1010 Fig. S12| Flow cytometry evaluation of subtypes of leukocytes in the pancreas of FM_{NC} and

1011 FM_{DSS} mice.

1012 Fig. S13| 0.2% DSS did not enrich bacteria in pacreas and disrupt the immune tolerance in

1013 antibiotic treated mice.

1014 Fig. S14| Identification of Muribaculaceae strain MF 13079.

1015 Fig. S15| Functional annotation of flagella-related genes and motility test of MF13079.

1016 Fig. S16| Bacteria load in mesenteric lymph nodes (MLN) in Akk and Muri mice.

1017 2. File name: Tables S1

1018 File Format: PDF

1019   Title and Discerption: Culture medium used for isolation of Muribaculeae

1020 3. File name: Tables S2

1021   File Format: Excel

1022   Title and Discerption: COG in the genome of MF 13079